Morphological, structural, electrical, and piezoelectric analysis of hydrothermally grown ZnO nanowires on various substrates

Abderrahmane Hamdi, Ahmad Hamieh, Mervat Alamri, Karim Dogheche, M.M. Saj Mohan, Rachel Desfeux, Denis Remiens, El Hadj Dogheche

Version of Record: https://www.sciencedirect.com/science/article/pii/S2468023022003716
Manuscript_7d2d7168fa791030d885df05d4398012

Morphological, structural, electrical, and piezoelectric analysis of hydrothermally grown ZnO nanowires on various substrates

Abderrahmane Hamdi [a *], Ahmad Hamieh [a], Mervat Alamri [a], Karim Dogheche [a], M. M. Saj Mohan [c], Rachel Desfeux [c], Denis Remiens [a, b], Elhadj Dogheche [a, b]

[a] *Université Polytechnique Hauts de France UPHF, IEMN DOAE UMR CNRS 8520, Valenciennes, France*

[b] *Institut d'électronique, de Microélectronique et de Nanotechnologie (IEMN), Université de Lille, CNRS, Centrale Lille, ISEN, Université de Valenciennes, UMR 8520 – IEMN, F-59000 Lille, France*

[c] *Univ. Artois, CNRS, Centrale Lille, Univ. Lille, UMR 8181, Unité de Catalyse et Chimie du Solide (UCCS), F-62300 Lens, France*

[*] Corresponding Author: Abderrahmane Hamdi; E-mail: Abderrahmane.Hamdi@uphf.fr,

Phone Number: +33783704486

Abstract

In this present work, we have successfully fabricated a piezoelectric structure based on ZnO nanowires (ZnO NWs) using a simple, low cost and environmentally friendly hydrothermal method. This structure forms the basis to fabricate vertically integrated nanogenerator device.

This paper attempts to study the effect of several parameters such as the seed layer morphology, seed layer roughness, seed layer annealing temperature, growth temperature, and growth time on three different substrates, which are silicon substrate with a gold & platinum film as lower metal contact, and stainless steel. The structure and morphology of the seed layer and the as-obtained nanowires were characterized using scanning electron microscopy (SEM), high-resolution transmission electron microscopy (HR-TEM), and X-ray diffraction (XRD). SEM analysis shows that the non-aqueous seed solution must be stirred to avoid the formation of the two phases (milky and translucid) and thus the formation of ZnO particles with different sizes and morphologies. In addition, the annealing temperature influences the diameter of the ZnO seed layer and thus ZnO nanowires diameter. This work also shows that the length of the nanowires increases with the growth duration without affecting ZnO diameter (70±30 nm). HR-TEM and XRD studies show the high crystalline quality of the one-dimensional nanomaterials deposited on stainless steel and confirm their high density along the c-axis direction. In this paper, we have also investigated the electrical and piezoelectric performances of the structure obtained. Indeed, the I-V curves exhibit nonlinear and asymmetric electrical characteristics, which confirms the formation of Schottky contacts between the metal and ZnO NWs. According to the piezo-response force microscope, an effective piezoelectric coefficient d33 between 5 and 7 pm/V as a function of the substrate was measured.

Keywords

ZnO nanowires; ZnO seeds; hydrothermal growth; characterizations; annealing temperature; piezoelectric structure

1. Introduction

Due to the increasing demand for eco-friendly materials, research on zinc oxide continues to interest scientists around the world. This inorganic compound has numerous advantages such as chemical stability, biocompatibility, eco-friendly, low-cost and easily synthesized, etc [1].

Zinc oxide can be obtained in different shapes and forms such as nanoparticles [2], nanosheets [3], nanoflowers [4], nanoflakes [5], nanowalls [6], nanorods [7], nanowires [8], and so on. Among these nanostructures, vertically aligned zinc oxide nanowires have attracted much attention due to their interesting properties. They are widely used for applications in field emission transistors, photodetectors [9], solar cells [10], water splitting [11], UV and blue light emitting diodes (LEDs) [12], nanogenerators [13], photocatalysis [14], gas sensors [15], preventing Marine Fouling [16], Self-cleaning [17], and so on.

Comparing ZnO nanowires to bulk ZnO and thin films, nanowires have less grain boundaries and defects. They have large surface-to-volume ratios and high active surface [18]. Moreover, they have efficient charge transport along the nanowire axis and the geometry of this nanostructured material exhibits strong confinement effect [19]. In addition, owing to its non-centrosymmetric structure, one of the important properties is their piezoelectricity which is extensively studied in theoretical and also in experimental.

Owing to the above-mentioned properties, a broad range of methods have been reported on the synthesis of ZnO nanostructures. Indeed, ZnO nanowires can be synthesized by several methods, such as vapour–liquid–solid (VLS) growth [20], electrochemical deposition [21], chemical vapour deposition (CVD) [22], ultrasonic spray pyrolysis technique [23], etc. However, the above-mentioned methods are usually operated at high temperature (>100 °C) and require sophisticated equipment. Therefore, the hydrothermal method has been reported as an alternative way to synthesize ZnO NWs. Owing to its simplicity, low-cost process, low temperature (<100 °C), scalable process, and high yield, numerous studies have been performed on the growth of ZnO nanowires using this technique [13].

Another advantage of this method is the possibility of using different types of substrates. Depending on the application, ZnO nanowires have been grown on both soft and hard substrates such as cotton fabrics [17], polymer [13], semiconductor [24], glass [25], and metal [7]. In order to grow one-dimensional nanomaterials on this wide variety of substrates, a seed layer of ZnO is required. This layer will act as nucleation sites, improve the alignment and the homogeneity of the nanowires, and reduce the lattice mismatch between the ZnO NWs and the substrates [26].

The aim of the research is to investigate some Metal – Film – Metal structures that are compatible with the field of transportation technology. Therefore, the objective is to attain a perfect vertically aligned nanowires allowing the implementation of sensors matrix for health monitoring (with defects detection) as well as for piezogenerator to provide some power to these sensors. While, some research has been carried out on ZnO nanowires, there is little published papers on the influence of the seed layer deposited on different substrates. Herein, we have studied the geometry and crystalline quality of different substrates in order to get the maximum physical effect. These results are original and further enrich previously published research on ZnO nanowires and offer several advantages in terms of understanding the role and effect of the seed layer to obtain well-aligned ZnO nanowires.

2. Materials and methods

2.1. Materials

Zinc acetate dihydrate ($Zn(OOCCH_3)_2\ 2H_2O$, 98%) and granulated sodium hydroxide (NaOH, 98%) (products used for seed layer). Zinc nitrate hexahydrate ($N_2O_6Zn\ 6H_2O$, 98%), and hexamethylenetetramine (HMTA, 99+%) (products used for hydrothermal growth) were purchased from Alfa Aesar. Acetone, ethanol, and methanol were supplied by Thermo fisher and they were used with analytical grade. Distilled water was used for the preparation of all solutions, and for cleaning the surfaces.

2.2. Methods

In this work, we compare the morphological, structural, electrical, and piezoelectric properties of three substrates. The first one is a silicon substrate with a gold deposition as lower metal contact. The second one is silicon with a platinum deposition as lower metal contact, and the third one is a conductive substrate (stainless steel), which does not require metallization.

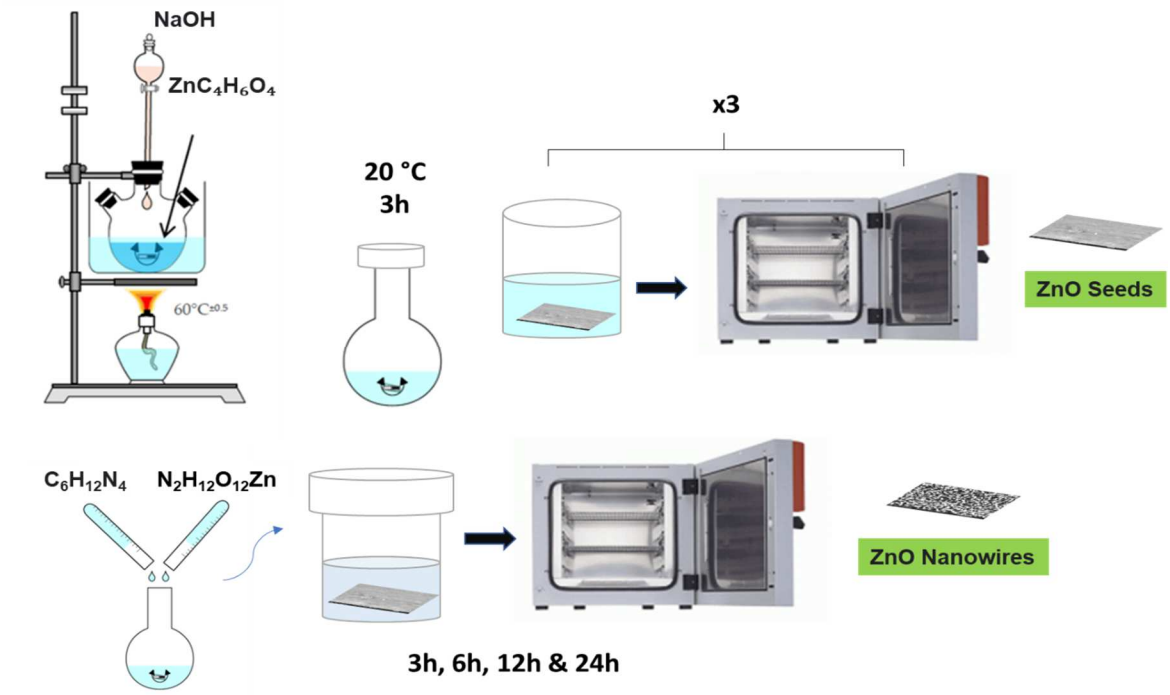

Fig. 1. Schematic illustration of ZnO nanowires array synthesis.

It should be noted that for silicon wafer, it was necessary to deposit a thin titanium (Ti) metal film to reduce the effect of lattice mismatch between the film and the substrate [26]. In addition, the Ti was deposited firstly on silicon to act as a glue layer between the substrate and the conductor layer. Xinghua Zhu et al, have shown that the mechanical stress attributed to the mismatch of lattice constant between the films and substrate, can cause film instability or even a film peeling [25].

Silicon wafer was used as a substrate with Ti/Au and Ti/Pt as bottom electrodes. The presence of these electrodes is necessary for electrical evaluations. However stainless steel was used as received. Interestingly, stainless steel is a conductive substrate that has better corrosion resistance, is readily available, and it can be recycled.

In order to obtain well reproducible layers, a rigorous preparation of the substrates was necessary. The substrates were cleaned in acetone, ethanol, and water (5 min each) in an ultrasonic bath then dried with nitrogen.

Note that the protocol for obtaining ZnO seed layer and ZnO Nanowires was based on that published by de Ali et al, but with some modifications [27]. Fig. 1 at the top shows the preparation of ZnO seeds. As we mentioned in the introduction, this layer will act as a germination layer. Indeed, zinc acetate and sodium hydroxide were dissolved separately in methanol under stirring for 15 min. Then, sodium hydroxide was added dropwise onto the zinc acetate at 60 ° C. Finally, the transparent seed solution was agitated for 3h at room temperature. The deposition of ZnO seeds on the substrates was performed by chemical bath deposition (CBD).

In fact, several techniques have already been used to deposit ZnO thin layer on substrates. We have selected the CBD method due to its advantages over others. It is simple to implement in experimental setups, low cost, large area production. In addition, it does not require high working pressure, nor sophisticated equipment. We need only the solution containing the precursors and the substrates [28].

Indeed, the substrates were immersed in the seed solution for 5 min. Then, they were dried at 120 °C for 10 min. Note that only one immersion was not sufficient to obtain a continuous film without holes. Therefore, this process was repeated three times to ensure uniform seed deposition. Finally, the coated substrates were annealed at 250 °C for 15 min which leads to the formation of ZnO nanocrystal seeds.

In the literature, Greene et al., have reported that annealed ZnO seed layer at 350 °C for 1 h on the hot plate produced the highest c-axis texturing of the film. This temperature will allow the solvent to evaporate and eliminate the organic residues. Subsequently, the decomposition temperature was lowered to 250 °C by Farhad et al., showing good c-axis texturing of ZnO seed layers [29].

For growing ZnO nanowires, aqueous solutions of zinc nitrate and hexamethylenetetramine in equimolar concentrations were mixed under stirring for 15 min. The three different substrates coated with ZnO nanocrystal seeds were subjected to a hydrothermal reaction. The growth duration was varied from 3 hours to 24 hours and the oven temperature was left constant equal to 90 °C. Note that 90 °C was chosen because it is the optimum growth temperature. A temperature less than 90 °C is insufficient to develop ZnO nanomaterials as explained in section 3.4. After the growth reaction, the substrates were removed, rinsed with water, and then dried. Fig. 1 at the bottom illustrates the ZnO NWs synthesis process. Fig. 2 shows the schematic diagram of ZnO nanowires grown on the three different substrates.

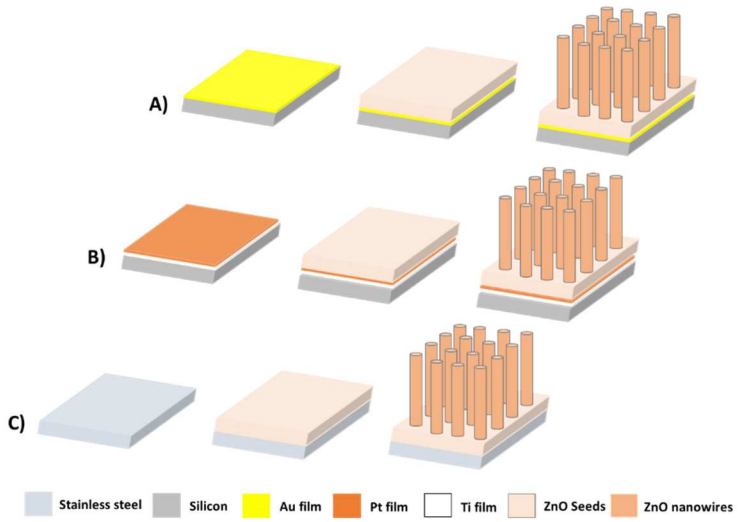

Fig. 2. Schematic diagram of the seed deposition and the hydrothermal growth of ZnO nanowires on different substrates.

2.3. Characterizations

In order to investigate the crystalline structure, the samples were analyzed by X-Ray Diffraction (XRD) by Siemens D5000 diffractometer, operating with Cu Kα radiation (λ = 1.5406 Å), an accelerating voltage of 40 kV, an applied current of 40 mA and 2θ of 20–60°.

The morphology of the ZnO nanowires was characterized using scanning electron microscopy (FEG–SEM, NEON 40 ZEISS) operating at 5 kV accelerating voltage.

The microstructures of ZnO NWs were observed using high-resolution transmission electron microscopy (HRTEM, JEOL JEM-2100F). Indeed, ZnO nanowires have been removed from the substrate and dispersed by sonication in isopropanol. After that, droplets of dispersed solution were dropped on a copper grid with carbon mesh.

For the investigation of electric properties, current-voltage (I–V) measurements were performed at room temperature by using Keithley Model 2450 Source Meter SMU Instrument.

Piezoresponse force microscopy (PFM) experiments were performed with an AFM microscope (MFP-3D, Asylum Research/Oxford Instruments, USA) operating at room temperature and under ambient conditions. Pt/Ir-coated conductive tips (nanosensors PPP-EFM probes with a nominal ~ 2.8 $N.m^{-1}$ spring constant) were used for measurement while the conductive substrate was grounded. To enhance the detected electromechanical signal, PFM analyses were carried out at the contact resonance frequency of the cantilever by using the Dual AC Resonance Tracking (DART) method [30].

3. Results and discussions

3.1. Effect of leaving the seed solution without agitation

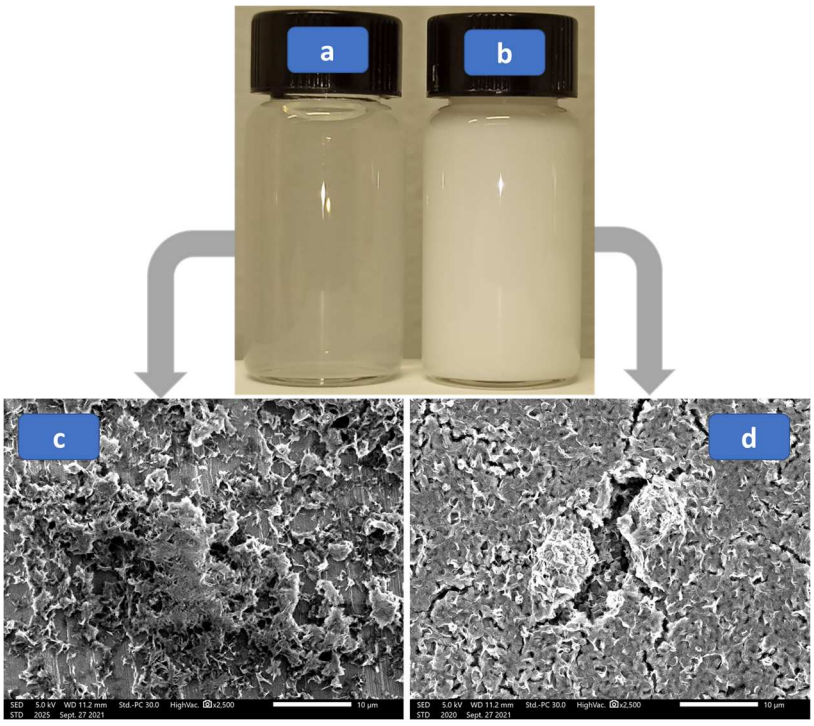

Fig. 3. Photo of the solution with the separated two phases and the corresponding SEM images after deposition on stainless steel.

In this study, we have performed several tests in order to observe the difference between the samples in terms of homogeneity and uniformity. We noticed that the deposited seed layer on the stainless-steel substrate and the growth thereafter appears more homogeneous than others. That is why some experiments were performed only on stainless steel. Several studies on ZnO nanowires have shown that the use of seed layers is important for growing these one-dimensional nanomaterials along the c axis, accordingly we have studied this layer from several aspects [31].

In this section, we noticed that not stirring the seed solution allows the formation of two phases, one translucent liquid (Fig. 3a) and the other one is solid formed by a white precipitate. By stirring this precipitate in the solution using an ultrasonic bath, a milky solution is obtained (Fig. 3b). Indeed, this solid phase consists of a high concentration of ZnO particles while the other phase is formed of less particles.

Figure 3.c shows that coating the stainless steel with the translucent solution enables the formation of heterogeneous layer. We can clearly see that the substrate is clearly visible under the discontinuous, porous, and randomly deposited ZnO film. While Figure 3.d shows that dispersing the high concentration of ZnO particles in the same solution and depositing it on the substrate permit the formation of thick ZnO layer. Moreover, this figure shows several cracks on the surface. Therefore, in order to obtain a homogeneous ZnO seed layer, the seed solution must be homogenous as well.

3.2. Effect of the seed layer roughness

Before growth	After growth
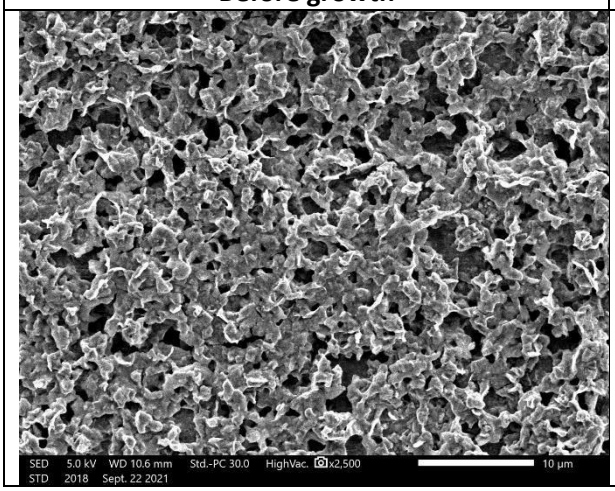	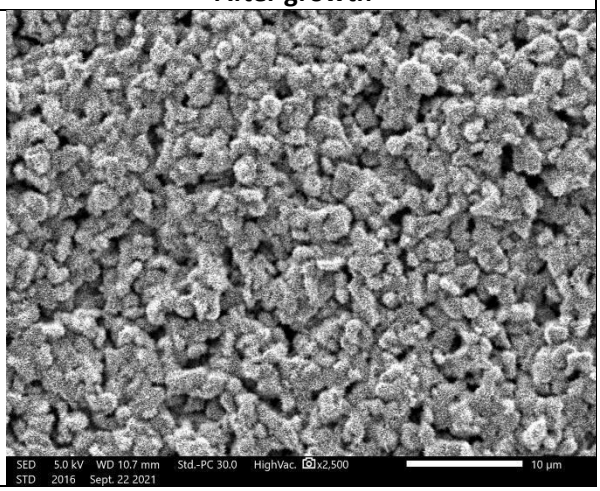

Fig. 4. Rough ZnO Seed layer deposited on stainless steel and the corresponding SEM image after the hydrothermal growth.

Fig. 4 presents a rough ZnO seed layer deposited on stainless steel by chemical bath deposition. As we can see, this layer is porous. It is formed by agglomeration and coalescence of microparticles. Growing ZnO nanowires on this layer allows the formation of a sea urchin-like structure, as we can observe in Fig. 4.

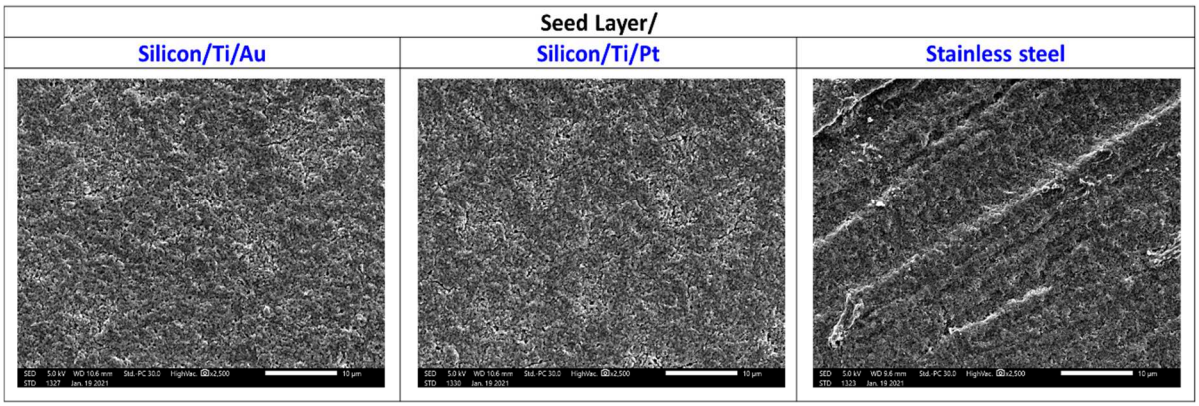

Fig.5. Top-view SEM images of ZnO Seeds deposited on the three different substrates.

Hence, we deposited ZnO seeds using a chemical bath deposition. It was performed thrice in order to obtain a uniform and homogeneous coating. SEM images of the surfaces after annealing the layers at 250 °C are shown in Fig. 5. We can clearly see that before the hydrothermal growth, top view images of the seeds layer deposited on the three different substrates exhibit almost the same nanostructure. In order to measure the thickness of the seed layer, a cross-sectional SEM image of the seed layers deposited on Pt/Ti/Silicon showed a thickness of about 600 nm.

In the present work, we did not examine the effect of the thickness of the ZnO seed layer. Indeed, the seed layer is important as a nucleation site for growing the nanowires. Likewise, the thickness of this buffer layer is also important as reported by many authors. Therefore, the effect of ZnO seed layer on the formation of ZnO nanowires will be investigated in more detail in our future work.

3.3. Effect of seed layer annealing temperature on the diameter of ZnO nanowires

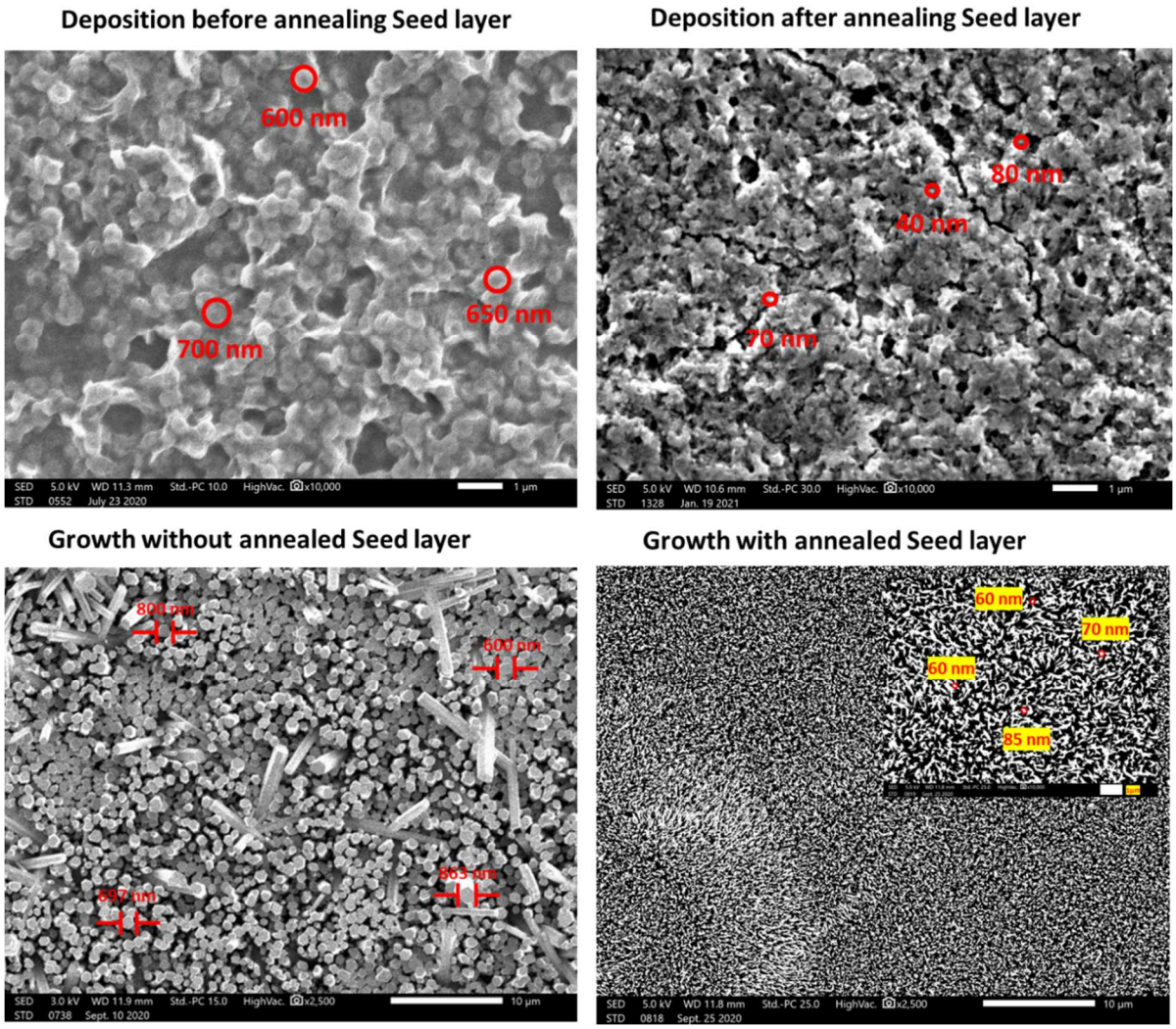

Fig. 6. SEM images showing the effect of seed layer annealing temperature on the diameter of ZnO nanowires.

Fig. 6 depicts the morphology of the seed layer with and without annealing at 250 °C and the corresponding SEM images after 24h of hydrothermal growth. It can be seen that the wire's diameters, forms, density, and length before annealing were different from those obtained after annealing. Therefore, this experiment highlights the effect of the seed layer annealing temperature to obtain either thick or fine nanowires.

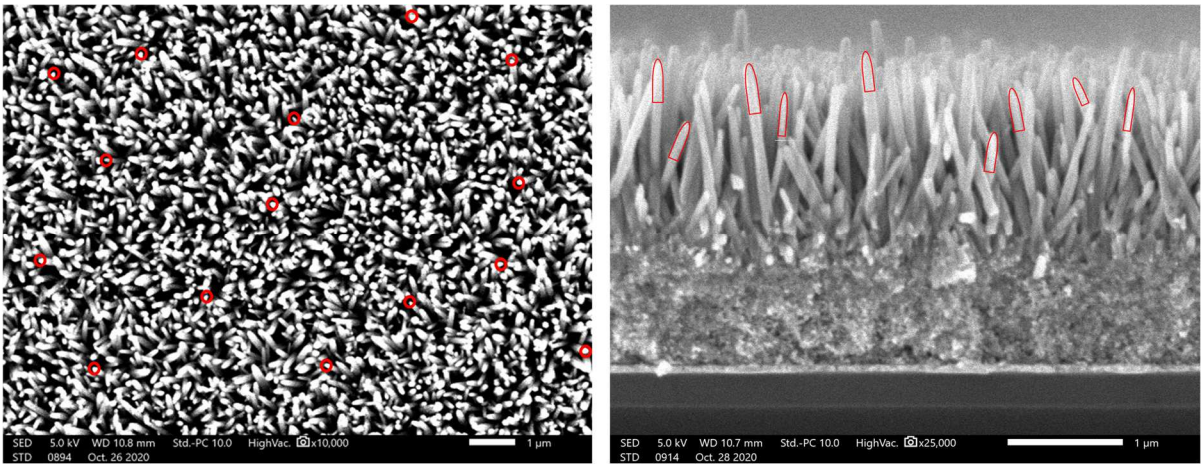

Fig. 7. Top view and side view SEM image of the top end of the nanowires.

In this work, most obtained 1-dimensional (1D) nanomaterials are nanowire-like structure. Fig.7 displays the ends of the nanowires, which present elliptic head shapes. They are not hexagonal and they show needle-like structure along [0 0 0 1]. However before annealing, these structures had a typical morphology of nanorods with hexagonal symmetry, and they are well faceted (Fig. 6). In the literature, there is no or little publications on both nanowires and nanorods [8]. Liu et al, reported that the main difference in morphology between ZnO nanowires and nanorods is that the nanowires do not have a hexagonal shape, unlike the nanorods [32].

Table 1: The average diameters of ZnO seeds and the nanowires grown on these seeds before and after annealing at 250°C.

Samples	**Average diameters (nm)**
Seed layer without annealing	700 ± 100
Seed layer with annealing	70 ± 30
ZnO nanowires grown on non-annealed seed layer	700 ± 100
ZnO nanowires grown on annealed seed layer	70 ± 30

The table below shows the average diameters of ZnO seeds and the nanowires grown on these seeds before and after annealing. As we can see from the table, the average diameter of ZnO NWs strongly depends on the seed layer annealing temperature. Indeed, we can clearly observe that ZnO nanowire diameter after annealing is 10 times lower than before annealing, it passes from 700 nm to less than 70 nm. Generally, increasing annealing temperature increases the grain size. However, the value of

this temperature is quite important. Yoon, Y.C., et al [33], reported that the thermal annealing between (100–300 °C) was not high enough to promote the coalescence of small grains. In addition, Guo, D et al [34], have shown that when ZnO thin films annealed at 250–350 °C, the films consisted of spherical grains. The annealing at 400 °C increases the grain size. Moreover, several authors have reported that ZnO films exhibit amorphous structure under 300 ℃ and even over 400 ℃ for others. On the other hand, the heating rate is very important. Hwang, K and co-authors [35], reported that the gel film has enough time to structurally relax before crystallization when the heating rate is low, resulting in denser ceramic films.

In our work, the formation of dense array ZnO nanowires with small diameter is due to the decomposition of zinc acetate and thus the formation of ZnO with small and denser grain sizes as explained by Hwang, K et al [35]. Accordingly, annealing at 250°C allows the formation of ZnO nanocrystals without their coalescence. Therefore, this experiment highlights the effect of the seed layer annealing temperature to obtain either thick or fine nanowires.

3.4. Effect of growth temperature on the formation of ZnO nanowires

In order to see the effect of temperature on the formation of aligned ZnO NWs, we have examined the three different samples at room temperature and at 90°C after 24h of growth, after annealing the seed layers at 250°C.

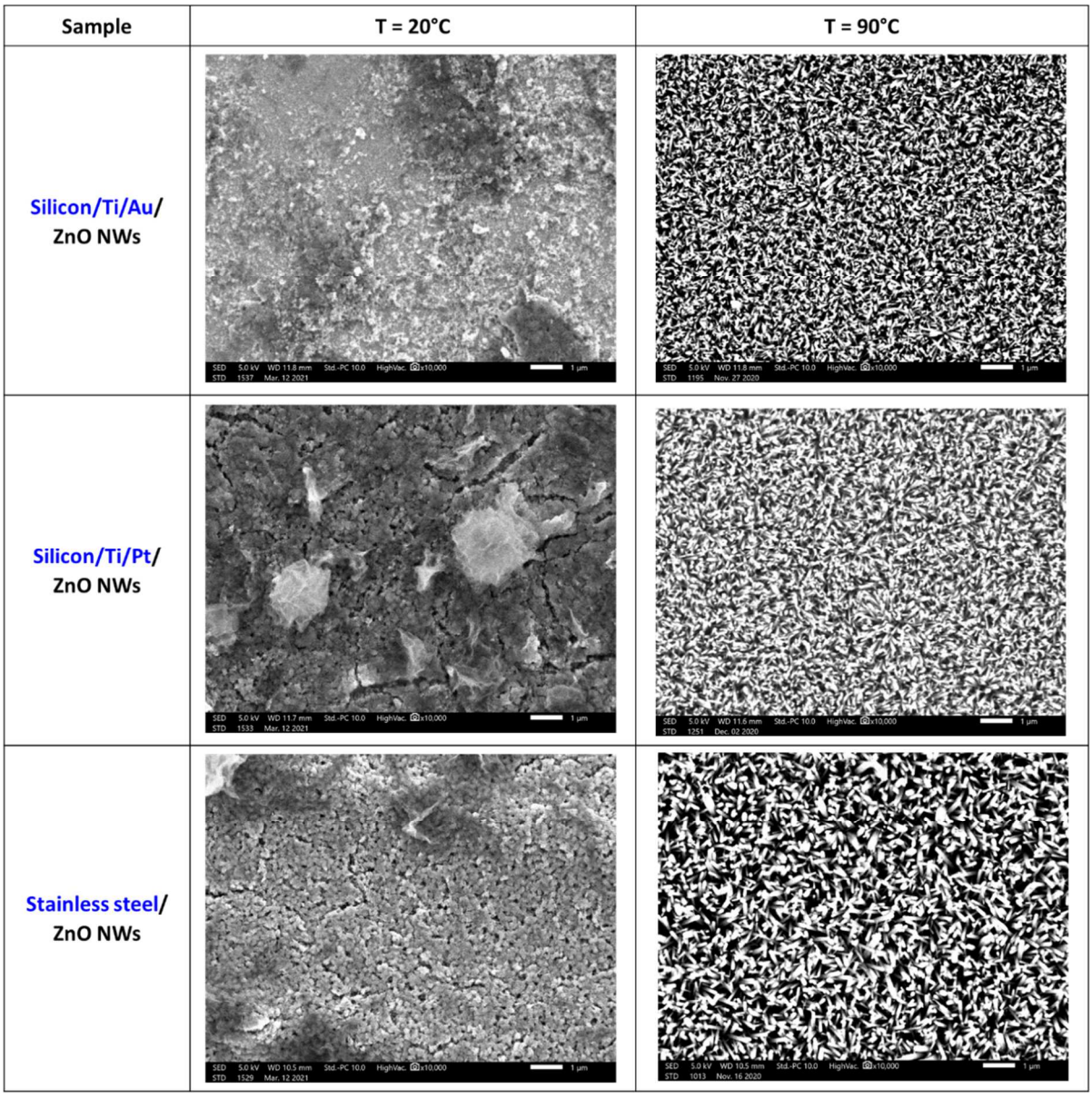

Fig. 8. The effect of growth temperature on the formation of ZnO nanowires hydrothermally grown on silicon/Ti/Au, silicon/Ti/Pt, and stainless steel.

SEM images in Fig. 8 clearly show that after the growth at room temperature, we didn't obtain ZnO NWs, unlike the growth at 90°C which shows that all the surfaces were covered by nanowires. Therefore, the growth temperature at 90 °C was kept constant for the rest of the experiments. In the literature, Kangeun Yoo et al. [31], have shown that lower temperatures (60-70 °C) were not sufficient to fully develop ZnO nanostructures. These structures begin to evolve into nanowires when the temperature increases to 80 ° C. Thereafter they choose 90 ° C as the optimum growth temperature, which leads to uniform and high dense nanowire arrays.

3.5. Growth time influences nanowire length

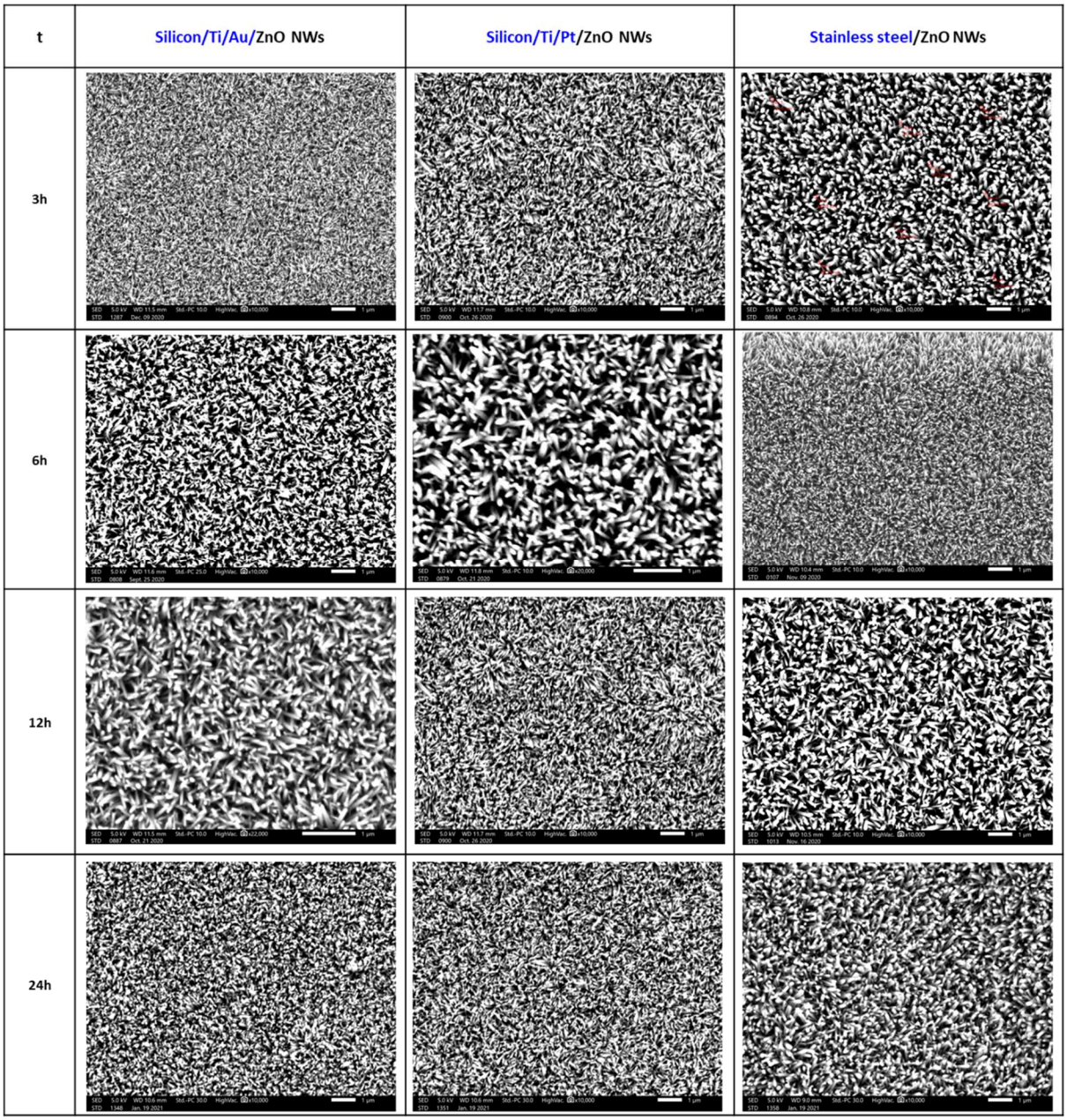

Fig. 9. Top-view SEM images of ZnO Seeds, ZnO nanowires that are grown at 90 °C for 3h, 6h, 12h, and 24h on the three different substrates. Bare scale 1 µm.

In this section, we have investigated the effect of the hydrothermal growth time on ZnO nanowire morphology while maintaining all other parameters constant.

After the growth at different durations 3, 6, 12, and 24h at 90°C, on the annealed seed layers, top-view SEM images are shown in Fig. 9. The nanowires were successfully grown homogeneously for all durations. We can clearly observe that dense arrays of ZnO NWs with diameter sizes about 70 ± 30

nm are formed on all substrates. The diameter of these nanowires is almost the same for all the surfaces. We can conclude that, with the increase of growth duration, the diameter remained constant. In addition, the density was almost the same. It is ultrahigh (25 nanowires/µm×µm).

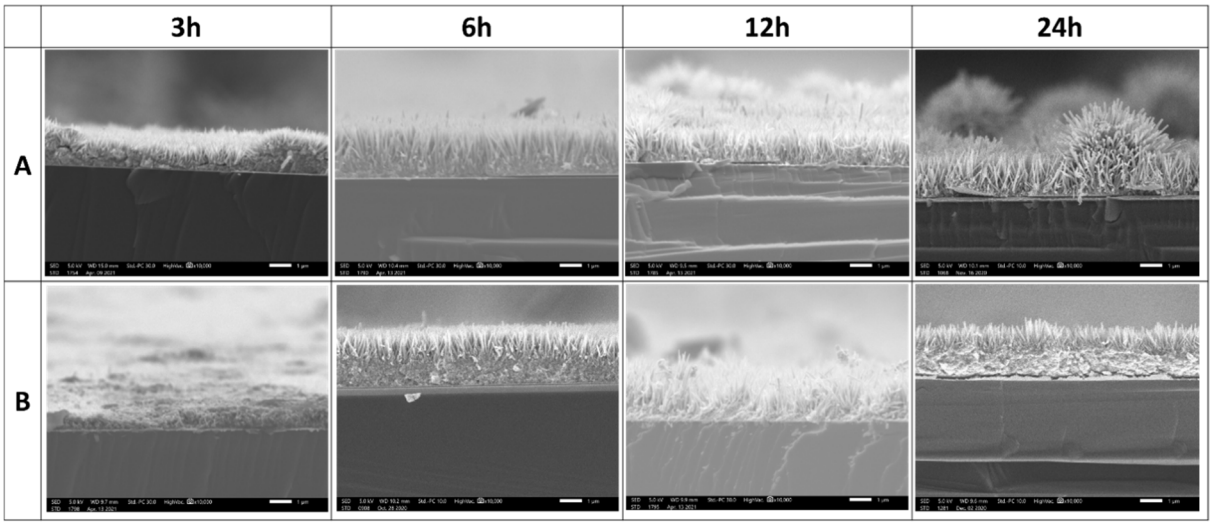

Fig. 10. Section-view SEM images of ZnO nanowires grown at 90 °C for 3h, 6h, 12h, and 24h on silicon/Ti/Au (labelled A in this table) and silicon/Ti/Pt (labelled B in this table).

In order to measure the length of the nanowires, a cross-sectional scanning electron microscopy of the substrates was performed. We note that cleaving silicon wafers is very easy, which allows cross-sectional observation, whereas on stainless steel it was not possible to perform this operation. Therefore, we could not measure the length of the nanomaterial on stainless steel and the cross-sectional images were performed only on ZnO NWs/Au/Silicon and ZnO NWs/Pt/Ti/Silicon. We found that the length increases with the growth duration time from 0.5 µm after 3h of growth to 1.5 µm after 24 h of growth. The images in Fig. 10 show an increase of ZnO NWs length with the growth duration without affecting the diameter. Indeed, the growth of the nanowires is therefore kinetically controlled by hexamine. This molecule controls the supply of OH- ions during growth. Additionally, it is revealed that HMTA would preferentially bind to the nonpolar facets of the ZnO nanowires, thus exposing only the (002) plane for epitaxial growth. In the literature, Vincenzina Strano et al. [36], have reported that beyond the well-established pH buffering activity, HMTA acts as capping agent promoting anisotropic growth via a steric hindrance effect, which inhibits the lateral growth of ZnO nanorods. Two years later, Parize, R et al. [37], have published on the multiple roles of HMTA in the

growth of ZnO nanowires. They have shown that this compound significantly reduces the radial growth of the nanowires by inhibiting the development of their non-polar m-plane sidewalls. Therefore, this experiment is interesting to study the length of nanowires as a function of the growth time.

3.6. Homogeneity of growth on different surfaces

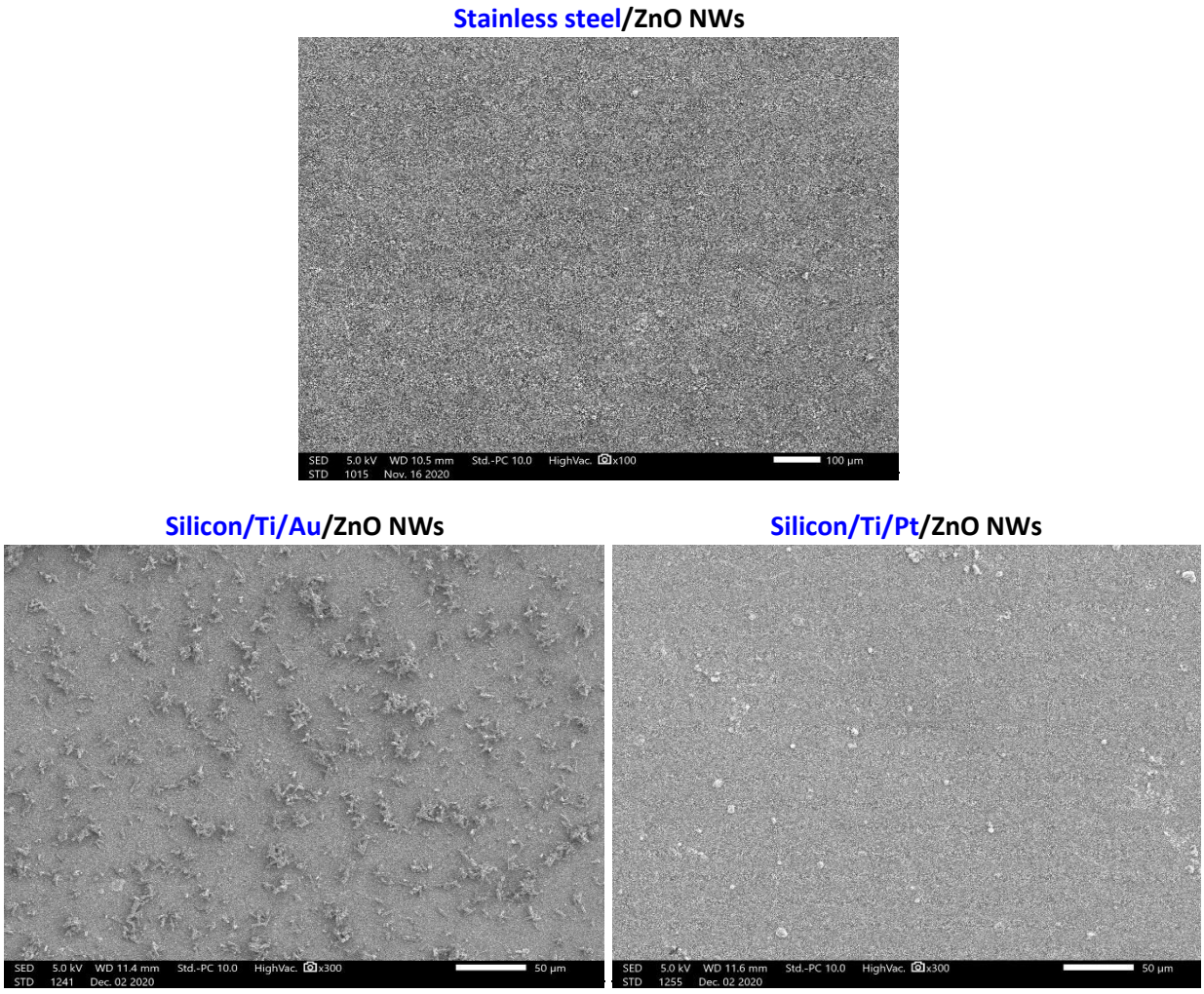

Fig. 11. Top-view SEM images showing the homogeneity of ZnO deposition on the different surfaces.

In this study, we have performed several tests in order to observe the difference between the samples in terms of homogeneity and uniformity. Indeed, before the SEM we noticed that the deposited seed layer on stainless-steel substrate and the growth thereafter appears visibly more homogeneous than others. In addition, the SEM image in Fig. 11, confirmed the visible observation, and the growth is always uniform whether on small or large stainless-steel surfaces.

However, concerning the other two substrates, we can clearly observe that especially for silicon/Ti/Au/ZnO NWs, the top-view SEM image shows that agglomerated particles and micro-wires are deposited on the annealed substrate at 250 ° C. This behavior could be attributed to the fact that on a gold film the formation of clusters can start from 150 ° C as reported by M S Rahman Khan [38]. These clusters will act as nuclei for ZnO nanowires which could explain the formation of aggregated ZnO microwires and microparticles on the surface. While on ZnO NWs/Pt/Ti/Silicon sample, we can see less aggregations on the surface. Indeed, authors have reported that platinum (Pt) does not adhere well to Si, SiO_2 or Si_3N_4. Therefore, a titanium thin layer is required to bond the metal to the material [39]. However, the poor thermal stability of the Pt/Ti electrode causes protruding grains, or hillocks on the surface. In our case, we have deposited TiO_x/Pt which greatly reduces the density of hillocks [40], and thus the agglomeration of particles and micro-wires as shown on the surface. This section highlights the advantages of using the stainless-steel substrate rather than coated silicon with gold or platinum to obtain homogeneous and well-aligned nanowires.

3.7. XRD and HR-TEM analysis

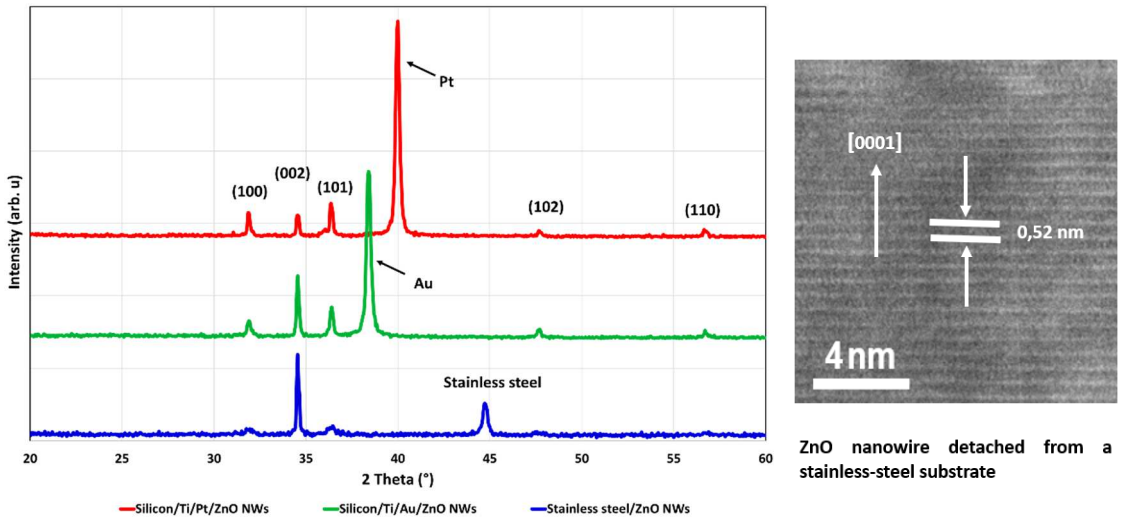

Fig. 12. X-ray diffraction (XRD) of the three different substrates after 24h of growth and high-resolution transmission electron microscopy (HR-TEM) image of ZnO nanowire detached from a stainless-steel substrate.

The crystallinity of ZnO nanowires was also evidenced by using X-ray diffraction (XRD). The XRD patterns of ZnO nanowire arrays grown on the three different substrates are shown in Fig. 12.

In the previous part, we have observed aggregated ZnO microwires and microparticles on silicon/Ti/Au/ZnO and Silicon/Pt/Ti. The nanowires were grown tilted and others deposited randomly on the surface, which could explain the polycrystalline structure of these two samples. However, for nanowires grown on stainless steel, the peak is strong and narrow compared to other samples, demonstrating a high degree of crystallinity of the prepared ZnO on this substrate. This could be attributed to the homogeneity and uniformity of the growth, as shown in Fig. 10. In addition, the nanowires arrays were vertically well-aligned to the surface.

In addition, the dominant diffraction peak at 2θ = 34.8° corresponding to (002) spacing of the wurtzite structure [Joint Committee on Powder Diffraction Standards (JCPDS) Card No: 05-0664, revealed a preferential alignment of the nanowires in their c-axis direction [41]. Furthermore, no diffraction peaks from Zn or other impurities are detected indicating the high purity of ZnO nanowires.

Fig. 12 also shows a high-resolution transmission electron microscopy image of ZnO nanowire after 24h of growth. The HR-TEM image shows that the crystal lattice fringes spacing are 0.52 nm which correspond to the d-spacing of the (0001) crystal planes [42]. This measured plane spacing shows that ZnO nanowire has a perfect lattice structure and confirms that they grow along the c-axis direction.

3.8. Electrical characterization

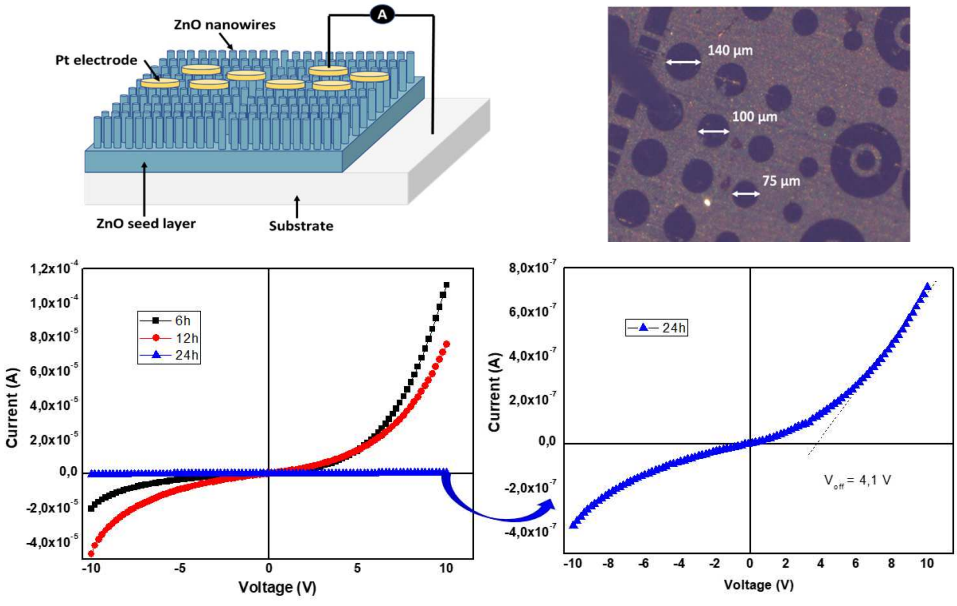

Fig. 13. Schematic illustration of ZnO nanowires-based nanogenerator, the microscope image of the deposited top-electrode (the area of the used electrode was 15393 μm^2), current−voltage characteristics (I−V) of ZnO nanowires grown at 6, 12, and 24h on stainless steel. The blue curve on the right corresponding to ZnO nanowires grown at 24 h, was magnified 10 times.

Optical image from Fig. 13 shows the deposited top-electrode on ZnO NWs. It can be seen that the electrodes have three different diameters, 75, and 100 and 140 µm. It is noteworthy that the electrical characteristics of the one-dimensional nanomaterials deposited on stainless steel were measured at room temperature and at atmospheric pressure. Therefore, the objective of this experiment is to confirm the Schottky behavior of the nanowires. Fig. 13 depicts the current−voltage characteristics (I−V) of ZnO NWs grown at 6, 12, and 24h. The measurements were performed by changing the DC bias from -10V to +10V. Indeed, by increasing the voltage, the emitted current increases, and the turn-on voltages are 6.3, 5.4 and 4.1 V after 6h, 12h, and 24h of growth, respectively. It can be seen clearly that the I-V curves present nonlinear and asymmetric electrical characteristics, which confirms the formation of Schottky contacts between the metal and the nanowires. Indeed, with short deposition times and therefore short nanowires, short-circuits or high leakage currents are very often observed. However, with long nanowires the effect is less marked. It is most certainly associated with the upper electrodes deposited directly on the nanowires and which is not the best configuration. The deposition of a polymer film between the nanowires and the upper electrode would eliminate or reduce this effect, as mentioned in the literature [43]. Further study on the type of deposition method and the high resistance of the nanowire-nanowire junction should be investigated in order to deposit an efficient top electrode.

3.9. Piezoresponse force microscopy (PFM) experiments

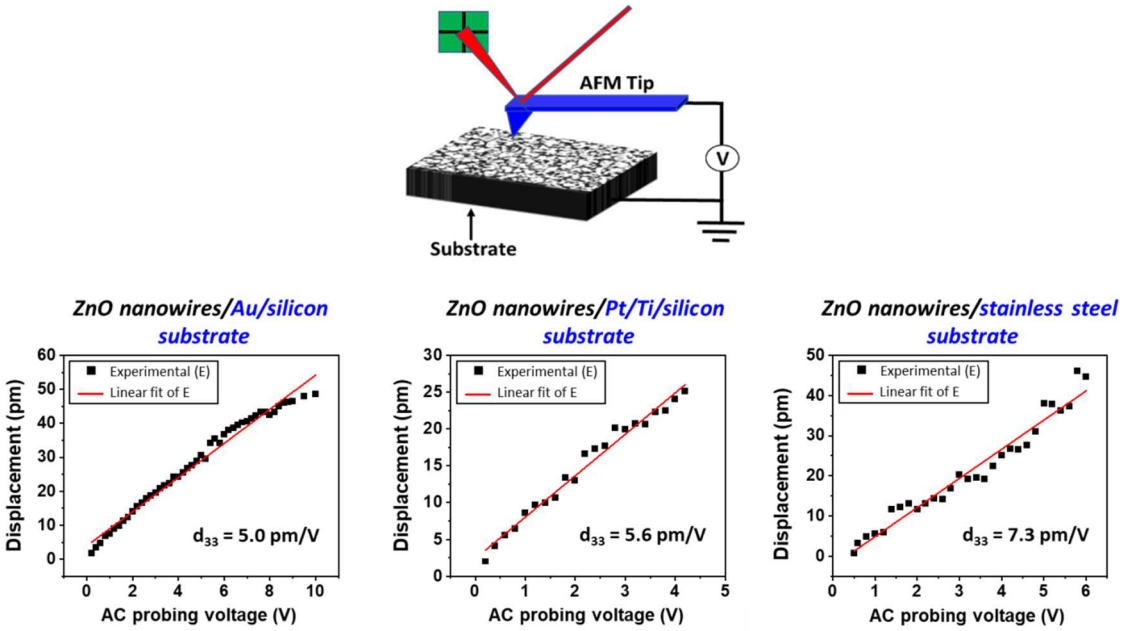

Fig. 14. Schematic of experimental set-up illustrating PFM measurements and the PFM displacement versus Vac driving voltage.

In our work, the determination of the piezoelectric properties of the vertically aligned ZnO nanowires grown on different substrates was performed using Piezoresponse-Force Microscopy. To do so, the effective piezoelectric coefficient d_{33} is investigated for the nanowires grown after 24hr of growth. To obtain quantitative values, the PFM probe was preliminary calibrated by using the GetReal function in the Asylum Research software to get inverse optical lever sensitivity (InvOLS) and spring constant of the cantilever at the same time. This is performed by scanning the thermal noise to get the resonance frequency of the cantilever when the tip is not in contact. Next, our reference sample [$Pb(Mg_{1/3}Nb_{2/3})O_3$-$PbTiO_3$ thin film] with known d_{33} piezoelectric constant is probed to quantify the performance of the PFM setup [44]. Keeping in mind that the detected signal amplitude A is amplified while operating at the contact resonance through the DART-PFM method, this requires take into consideration the quality factor Q in the relation $A = d_{33} \times V_{ac} \times Q$ (Q is about 100 for such ZnO hard material). The conductive tip was put into contact with the top of these vertically

aligned/grown nanowires to measure the piezoresponse amplitude signal. After establishing the contact resonance with the different ZnO nanowire samples, while a controlled constant force applied between the tip and these samples, the displacement values are recorded by sweeping the AC probe voltage [45,46]. The d_{33} values were then determined by considering the slope on the displacement versus AC probe voltage plot. Fig. 14 shows that d_{33} of the ZnO NWs deposited on stainless steel is about 7.3 pm/V. In order to measure the piezoresponse amplitude signal, the PFM conductive tip was put in contact with the top of these nanowires. Since the nanowires deposited on the stainless steel were vertically aligned on the surface and they were also highly crystalline, this could explain the fact that the piezoelectric coefficient of stainless steel is higher compared to others. This result makes it possible to use ZnO nanowires grown on stainless steel to design and fabricate next generation sensors and actuators in several fields, notably in transport.

The obtained values of the piezoelectric coefficient d_{33} on ZnO nanowires was close to that of bulk ZnO (d_{33} = 9.93 pm/V) [47]. This piezoelectric coefficient is still less than PZT-based nanomaterials nevertheless doping these nanowires would be a solution to reach high piezoelectric properties. In the literature, Nidhi Sinha et al., have shown that a gigantic piezoelectric coefficient (d_{33} > 400 pm/V) was obtained for yttrium-doped ZnO nanosheets [48].

4. Conclusion

In this study, we have successfully fabricated a piezoelectric structure based on ZnO nanowires using a simple, low cost and environmentally friendly method. The procedure was carried out on various substrates via hydrothermal growth where the effect of various parameters allowing the formation of aligned ZnO NWs has been investigated. We found that the seed solution should be agitated to avoid the formation of two phases (translucid and milky). The deposition of the translucid solution on the substrate showed discontinuous, porous, and randomly deposited ZnO film while the milky solution showed a thick ZnO layer allowing the formation of cracks on the surface. In addition, when the growth is conducted on agglomerated, coalesced microparticles, and sea urchins-like structures are formed. However, when a smooth seed layer is used, well-aligned ZnO nanowires are obtained. It

was also found that annealing temperature influences the diameter of ZnO seed layer and, thus ZnO nanowires diameter. This work has also shown that the length of the nanowires increases with the duration of growth without affecting the diameter (sizes in the range of 70 ± nm) as well as the diameter with the temperature. Furthermore, HR-TEM image shows the high crystalline quality of the nanowires deposited particularly on stainless steel and confirms their high density along the c-axis direction. On the other hand, XRD study confirmed the hexagonal wurtzite structure of ZnO nanowire arrays.

Based on the electrical characterization, the I-V curves exhibit nonlinear and asymmetric electrical characteristics, which confirms the formation of Schottky contacts between the platinum and ZnO nanowires. Finally, the piezo-response force microscope revealed that the piezoelectric activity of ZnO nanowires deposited on stainless steel has a coefficient d_{33} about 7.3 pm/V.

The results reported in this work have shown that the growth of ZnO nanowires on stainless steel is better in terms of homogeneity, uniformity, and piezoelectric response compared to silicon/Ti/Au and silicon/Ti/Pt. We believe that our study would be useful in obtaining high-quality, well-oriented, and high-density ZnO nanowires that can be used in different applications, including energy harvesting.

CRediT authorship contribution statement

Abderrahmane Hamdi: Characterization analysis and Writing-Original draft. Ahmad Hamieh: Methodology and Characterization analysis. Mervat Alamri: Sample preparation. Karim Dogheche: XRD measurement. M. M. Saj Mohan and Rachel Desfeux: PFM measurement. Denis Remiens and Elhadj Dogheche: Review and editing.

Funding

This work is supported by the Université Polytechnique Hauts-de-France (UPHF) under the Competitive Research Programs (Grant n°15-2021).

Conflicts of Interest

The authors declare that they have no known competing financial interests or personal relationships that could have appeared to influence the work reported in this paper.

Acknowledgments

The authors would like to acknowledge the platform FUMAP at IEMN DOAE for providing the facilities necessary for conducting the research.

Chevreul Institute (FR 2638), Ministère de l'Enseignement Supérieur, de la Recherche et de l'Innovation Région Hauts-de-France and FEDER are also acknowledged for funding the MFP-3D microscope under Program "Chemistry and Materials for a Sustainable Growth". Hauts-de-France Region, Fonds Européen de Développement Régional (FEDER) and Major Domain of Interest (DIM) "Eco-Energy Efficiency" of Artois University are acknowledged for supporting and funding partially this work.

References

[1] V.N. Kalpana, V. Devi Rajeswari, A review on green synthesis, biomedical applications, and toxicity studies of ZnO NPs, Bioinorganic Chemistry and Applications. 2018 (2018).

[2] H.B. Hadjltaief, S.B. Ameur, P. Da Costa, M.B. Zina, M.E. Galvez, Photocatalytic decolorization of cationic and anionic dyes over ZnO nanoparticle immobilized on natural Tunisian clay, Applied Clay Science. 152 (2018) 148–157.

[3] M.N. Rezaie, S. Mohammadnejad, S. Ahadzadeh, The impact of ZnO nanotube on the performance of hybrid inorganic/organic light-emitting diode as a single-mode ring-core UV waveguide, Surfaces and Interfaces. 28 (2022) 101666.

[4] A.J. Haider, F.I. Sultan, A. Al-Nafiey, Controlled growth of different shapes for ZnO by hydrothermal technique, in: AIP Conference Proceedings, AIP Publishing LLC, 2018: p. 030085.

[5] A. Sholehah, D.F. Faroz, N. Huda, L. Utari, N.L.W. Septiani, B. Yuliarto, Synthesis of ZnO flakes on flexible substrate and its application on ethylene sensing at room temperature, Chemosensors. 8 (2020) 2.

[6] B. El Zein, S. Boulfrad, G.E. Jabbour, E. Dogheche, Parametric study of self-forming ZnO Nanowall network with honeycomb structure by Pulsed Laser Deposition, Applied Surface Science. 292 (2014) 598–607.

[7] A. Alshehri, P. Champagne, L. Keirsbulck, E.H. Dogheche, Nanotechnology to improve the performances of hydrodynamic surfaces, Coatings. 9 (2019) 808.

[8] L. Vayssieres, Growth of arrayed nanorods and nanowires of ZnO from aqueous solutions, Advanced Materials. 15 (2003) 464–466.

[9] C.-L. Hsu, S.-J. Chang, Y.-R. Lin, P.-C. Li, T.-S. Lin, S.-Y. Tsai, T.-H. Lu, I.-C. Chen, Ultraviolet photodetectors with low temperature synthesized vertical ZnO nanowires, Chemical Physics Letters. 416 (2005) 75–78.

[10] B.L. Muhammad, F. Cummings, Nitrogen plasma treatment of ZnO and TiO2 nanowire arrays for polymer photovoltaic applications, Surfaces and Interfaces. 17 (2019) 100382.

[11] P. Batista-Grau, R. Sánchez-Tovar, R.M. Fernández-Domene, J. Garcia-Anton, Formation of ZnO nanowires by anodization under hydrodynamic conditions for photoelectrochemical water splitting, Surface and Coatings Technology. 381 (2020) 125197.

[12] P. Yang, H. Yan, S. Mao, R. Russo, J. Johnson, R. Saykally, N. Morris, J. Pham, R. He, H.-J. Choi, Controlled growth of ZnO nanowires and their optical properties, Advanced Functional Materials. 12 (2002) 323–331.

[13] T. Slimani Tlemcani, C. Justeau, K. Nadaud, G. Poulin-Vittrant, D. Alquier, Deposition time and annealing effects of ZnO seed layer on enhancing vertical alignment of piezoelectric ZnO nanowires, Chemosensors. 7 (2019) 7.

[14] L. Roza, V. Fauzia, M.Y. Abd Rahman, Tailoring the active surface sites of ZnO nanorods on the glass substrate for photocatalytic activity enhancement, Surfaces and Interfaces. 15 (2019) 117–124.

[15] O. Lupan, G.A. Emelchenko, V.V. Ursaki, G. Chai, A.N. Redkin, A.N. Gruzintsev, I.M. Tiginyanu, L. Chow, L.K. Ono, B.R. Cuenya, Synthesis and characterization of ZnO nanowires for nanosensor applications, Materials Research Bulletin. 45 (2010) 1026–1032.

[16] J. Wang, S. Lee, A.R. Bielinski, K.A. Meyer, A. Dhyani, A.M. Ortiz-Ortiz, A. Tuteja, N.P. Dasgupta, Rational Design of Transparent Nanowire Architectures with Tunable Geometries for Preventing Marine Fouling, Advanced Materials Interfaces. 7 (2020) 2000672.

[17] M. Ashraf, P. Champagne, C. Campagne, A. Perwuelz, F. Dumont, A. Leriche, Study the multi self-cleaning characteristics of ZnO nanorods functionalized polyester fabric, Journal of Industrial Textiles. 45 (2016) 1440–1456.

[18] E. Muchuweni, T.S. Sathiaraj, M.T. Magama, P. Dzomba, Effect of annealing on the optical constants of ZnO nanowires for energy harvesting applications, Journal of Optoelectronics and Advanced Materials. 22 (2020) 200–204.

[19] J. Cui, Zinc oxide nanowires, Materials Characterization. 64 (2012) 43–52.

[20] M.-H. Zhao, Z.-L. Wang, S.X. Mao, Piezoelectric characterization of individual zinc oxide nanobelt probed by piezoresponse force microscope, Nano Letters. 4 (2004) 587–590.

[21] H. Zeng, J. Cui, B. Cao, U. Gibson, Y. Bando, D. Golberg, Electrochemical deposition of ZnO nanowire arrays: organization, doping, and properties, Science of Advanced Materials. 2 (2010) 336–358.

[22] S. Ma, A.H. Kitai, Chemical vapor deposition-based growth of aligned ZnO nanowires on polycrystalline Zn 2 GeO 4: Mn substrates, Journal of Materials Science. 52 (2017) 9324–9334.

[23] M.T. Htay, Y. Hashimoto, Field emission property of ZnO nanowires prepared by ultrasonic spray pyrolysis, Superlattices and Microstructures. 84 (2015) 144–153.

[24] B. ElZein, Y. Yao, A.S. Barham, E. Dogheche, G.E. Jabbour, Toward the Growth of Self-Catalyzed ZnO Nanowires Perpendicular to the Surface of Silicon and Glass Substrates, by Pulsed Laser Deposition, Materials. 13 (2020) 4427.

[25] X. Zhu, P. Gu, H. Wu, D. Yang, H. Sun, P. Wangyang, J. Li, H. Tian, Influence of substrate on structural, morphological and optical properties of TiO2 thin films deposited by reaction magnetron sputtering, Aip Advances. 7 (2017) 125326.

[26] E. Muchuweni, T.S. Sathiaraj, H. Nyakotyo, Low temperature synthesis of ZnO nanowires on GAZO thin films annealed at different temperatures for solar cell application, Materials Science in Semiconductor Processing. 68 (2017) 80–86.

[27] N.A. Alshehri, A.R. Lewis, C. Pleydell-Pearce, T.G. Maffeis, Investigation of the growth parameters of hydrothermal ZnO nanowires for scale up applications, Journal of Saudi Chemical Society. 22 (2018) 538–545.

[28] A. Kassim, T.W. Tee, H.S. Min, S. Monohorn, S. Nagalingam, Effect of bath temperature on the chemical bath deposition of PbSe thin films, Kathmandu University Journal of Science, Engineering and Technology. 6 (2010) 126–132.

[29] S. Rajamanickam, S.M. Mohammad, Z. Hassan, Effect of zinc acetate dihydrate concentration on morphology of ZnO seed layer and ZnO nanorods grown by hydrothermal method, Colloid and Interface Science Communications. 38 (2020) 100312.

[30] B.J. Rodriguez, C. Callahan, S.V. Kalinin, R. Proksch, Dual-frequency resonance-tracking atomic force microscopy, Nanotechnology. 18 (2007) 475504.

[31] K. Yoo, W. Lee, K. Kang, I. Kim, D. Kang, D.K. Oh, M.C. Kim, H. Choi, K. Kim, M. Kim, Low-temperature large-area fabrication of ZnO nanowires on flexible plastic substrates by solution-processible metal-seeded hydrothermal growth, Nano Convergence. 7 (2020) 1–10.

[32] F. Liu, P.J. Cao, H.R. Zhang, C.M. Shen, Z. Wang, J.Q. Li, H.J. Gao, Well-aligned zinc oxide nanorods and nanowires prepared without catalyst, Journal of Crystal Growth. 274 (2005) 126–131.

[33] Y.-C. Yoon, K.-S. Park, S.-D. Kim, Effects of low preheating temperature for ZnO seed layer deposited by sol–gel spin coating on the structural properties of hydrothermal ZnO nanorods, Thin Solid Films. 597 (2015) 125–130.

[34] D. Guo, K. Sato, S. Hibino, T. Takeuchi, H. Bessho, K. Kato, Low-temperature preparation of (002)-oriented ZnO thin films by sol–gel method, Thin Solid Films. 550 (2014) 250–258.

[35] K. Hwang, Y. Lee, S. Hwangbo, Growth, structure and optical properties of amorphous or nano-crystalline ZnO thin films prepared by prefiring-final annealing, Journal of Ceramic Processing Research. 8 (2007) 305.

[36] V. Strano, R.G. Urso, M. Scuderi, K.O. Iwu, F. Simone, E. Ciliberto, C. Spinella, S. Mirabella, Double role of HMTA in ZnO nanorods grown by chemical bath deposition, The Journal of Physical Chemistry C. 118 (2014) 28189–28195.

[37] R. Parize, J. Garnier, O. Chaix-Pluchery, C. Verrier, E. Appert, V. Consonni, Effects of hexamethylenetetramine on the nucleation and radial growth of ZnO nanowires by chemical bath deposition, The Journal of Physical Chemistry C. 120 (2016) 5242–5250.

[38] M.R. Khan, Hillock and island formation during annealing of gold films, Bulletin of Materials Science. 9 (1987) 55–60.

[39] N. Maluf, K. Williams, An introduction to microelectromechanical systems engineering, Artech House, 2004.

[40] J.-L. Cao, A. Solbach, U. Klemradt, T. Weirich, J. Mayer, H. Horn-Solle, U. Böttger, P.J. Schorn, T. Schneller, R. Waser, Structural investigations of Pt⁄ Ti O x electrode stacks for ferroelectric thin film devices, Journal of Applied Physics. 99 (2006) 114107.

[41] Y. Zhang, M.K. Ram, E.K. Stefanakos, D.Y. Goswami, Synthesis, characterization, and applications of ZnO nanowires, Journal of Nanomaterials. 2012 (2012).

[42] S.-N. Bai, T.-Y. Tseng, The structural and optical properties of ZnO nanowire arrays prepared by hydrothermal synthesis method, Journal of Materials Science: Materials in Electronics. 20 (2009) 604–608.

[43] C. Opoku, A.S. Dahiya, C. Oshman, F. Cayrel, G. Poulin-Vittrant, D. Alquier, N. Camara, Fabrication of ZnO nanowire based piezoelectric generators and related structures, Physics Procedia. 70 (2015) 858–862.

[44] A. Ferri, F. Rault, A. Da Costa, C. Cochrane, M. Boudriaux, G. Lemort, C. Campagne, E. Devaux, C. Courtois, R. Desfeux, Local electrical characterization of PVDF textile filament, Fibers and Polymers. 20 (2019) 1333–1339.

[45] T. Li, Y.T. Li, W.W. Qin, P.P. Zhang, X.Q. Chen, X.F. Hu, W. Zhang, Piezoelectric size effects in a zinc oxide micropillar, Nanoscale Research Letters. 10 (2015) 1–7.

[46] H.D. Espinosa, R.A. Bernal, M. Minary-Jolandan, A review of mechanical and electromechanical properties of piezoelectric nanowires, Advanced Materials. 24 (2012) 4656–4675.

[47] A. Quintana Romero, A. Gómez, M.D. Baró, S. Suriñach, E.M. Pellicer Vilà, J. Sort Viñas, Self-templating faceted and spongy single-crystal ZnO nanorods: resistive switching and enhanced piezoresponse, (2017).

[48] N. Sinha, S. Goel, A.J. Joseph, H. Yadav, K. Batra, M.K. Gupta, B. Kumar, Y-doped ZnO nanosheets: Gigantic piezoelectric response for an ultra-sensitive flexible piezoelectric nanogenerator, Ceramics International. 44 (2018) 8582–8590.